Mon. Not. R. astr. Soc. (1992) **255**, 471–485

Direct diagnosis of infall in collapsing protostars – I. The theoretical identification of molecular species with broad velocity distributions

J. M. C. Rawlings,[1,2] T. W. Hartquist,[1] K. M. Menten[3] and D. A. Williams[4]

[1] *Max Planck Institute for Extraterrestrial Physics, 8046 Garching, Germany*
[2] *Department of Physics, Astrophysics, University of Oxford, Nuclear Physics Laboratory, Keble Road, Oxford OX1 3RH*
[3] *Harvard-Smithsonian Center for Astrophysics, 60 Garden Street, Cambridge, MA 02138, USA*
[4] *Department of Mathematics, UMIST, PO Box 88, Manchester M60 1QD*

Accepted 1991 November 1. Received 1991 October 17; in original form 1991 July 24

SUMMARY

We have developed chemical models, including depletion on to grains, for the collapsing envelopes of protostars. Our primary goal has been to identify molecular species having broad velocity distributions, so that observations of their line profiles can be employed to diagnose the dynamics of protostar formation, and to yield information on the collapse age and depletion rate. Previously obtained data for NH_3 emission lines, from a number of dark cores with embedded protostars, have shown no clear evidence for systematic collapse. Results from our model indicate that the collapse initiates very soon after the formation of an isothermal pressure-balanced sphere. The collapse is preceded by a period of exceptional quiescence. We demonstrate here that as depletion reduces the fractional abundance of NH_3 in the accelerating gas of an infalling envelope and prevents the formation of broad wings on NH_3 emission lines, the fractional abundances of some other species initially increase as the heavy elements become depleted, leading those species to have emission lines broader than those of NH_3. CH is an observable species which, for a large variety of conditions, possesses a fairly constant or increasing fractional abundance in collapsing envelope gas in which depletion is occurring. High angular resolution observations of CH would be very desirable, but would require appropriate instrumentation on an array, or perhaps the Arecibo telescope. When the water abundance is sufficiently high in the outer envelope, so that many molecular ions are removed primarily in reactions with it rather than by dissociative recombination, the abundances of HCO^+, N_2H^+ and H_2S rise when collapse and depletion occur. Millimetre lines from these species can be observed with single-dish telescopes at higher angular resolution than can NH_3, resulting in their lines having broader wings in spatially resolved sources than those of NH_3, even when their abundances relative to NH_3 do not increase substantially in the infall. HCO is a particularly interesting species, because its abundance ratio relative to HCO^+ increases with growing density if the fractional abundance of gas-phase heavy metals remains constant. Also, HCO line emission can be observed with high angular resolution.

1 INTRODUCTION

High spectral resolution observations of dark ('dense core') globules have not provided clear evidence for infall, even when they possess embedded low-mass protostars or young stellar objects. This is curious because infall might be expected to continue until the protostellar winds begin to affect the dynamics of the globules.

Specifically, the (1,1) and (2,2) transitions of NH_3 (at 1.3 cm) have been mapped in B335 by Menten *et al.* (1984), in L1551 by Menten & Walmsley (1985) and in 27 globules including L1498, by Myers & Benson (1983).

Like most of the objects observed by Myers & Benson, L1498 is a low-mass (0.36 $M_\odot$), uniformly cold (10 K), low-density ($\sim 10^4$ cm^{-3}) roughly spherical globule with a radius of about 0.063 pc. The measured line profile for L1498 was

compared by Myers & Benson to a theoretical profile, calculated under the assumptions that the fractional abundance, $x(NH_3)$, of NH_3 is constant throughout the globule, and that the velocity and density structures are given by the theoretical protostellar collapse calculations of Larson (1972) for the time at which about half of the collapsing globule is concentrated in the protostellar nucleus. They found that the observed profile is substantially narrower than the model predicts and does not exhibit any noticeable high-velocity wings. Indeed, the profile is only marginally wider than that of a static cloud at $T=10$ K. This slight difference was attributed either to subsonic microturbulence or to collapse in a very early stage of development. The possibility of rotational broadening was observationally excluded.

The study by Menten *et al.* (1984) of NH_3 in B335, an 'isolated' dark globule of 27 $M_\odot$ and containing a compact far-infrared source, provided further information. They simultaneously observed the NH_3 (1,1) and (2,2) lines and were thus able to calculate the NH_3 rotation temperature, which was found to be constant at 10–12 K throughout the globule. Menten *et al.* also pointed out that the globule appears unusually quiescent, (an important point of the model we describe). They hypothesized that the freeze-out of ammonia on to dust grains gives rise to a significant depletion in the NH_3 fractional abundance in higher density flowing gas, and prevents the details of the NH_3 line profiles from properly reflecting the dynamics.

Though the NH_3 gas-phase abundance does decline with increasing depletion, some gas-phase molecular abundances actually increase as depletion occurs. In particular, the CH abundance is expected to rise with moderate depletion (Hartquist & Williams 1989), and it and other species might be expected to have lines possessing detectable high-velocity wings formed in infalling gas, even if NH_3 does not.

The observation of broad wings of suitable emission lines would constitute a powerful probe into the dynamics within a globule. By comparing line profiles of different species, we would be able to obtain information about depletion rates, the mass of the protostellar object, the age of the collapse, and the detailed dynamics of the collapse.

Our objective is to identify lines that are likely to have broad wings emitted in infalling gas in the envelopes of protostars. We have adopted a reasonable description of the dynamics of globule formation and collapse to form a protostar, and have followed the chemical evolution, including depletion, in each of a large number of parcels of gas in that globule. By following the chemistry, we were able to calculate the velocity distribution of molecular species and discover which have emission lines with high-velocity wings.

In Section 2, we summarize the assumed dynamical description. Section 3 contains a discussion of details of the chemical model. Section 4 is a presentation of results, and in Section 5 we give conclusions.

2 THE DYNAMICAL MODEL

2.1 General description

We found that the NH_3 fractional abundances of about 10^{-7} measured for many of the observed globules could not be produced by the gas-phase chemical scheme that we used. Like Nejad, Williams & Charnley (1990) we suggest that the large gas-phase abundances of NH_3 arise because it is injected from grains, on which much of the nitrogen is chemically processed to form NH_3, sputtered in shocks associated with the dynamical cycling (Norman & Silk 1980; Goldsmith, Langer & Wilson 1986) occurring in regions of low-mass star formation. The chemistry associated with such dynamical cycling and the physics of stellar-wind–globule interfaces have been considered by Williams & Hartquist (1984), Charnley *et al.* (1988a,b, 1990) and Nejad *et al.* (1990). In previous work, the cooled postshock gas, rich in material sputtered from the grains, consists of a decelerated mixture of stellar wind and material ablated from the globule, and comprises an interglobule medium having a number density of hydrogen nuclei, $n=n(H)+2n(H_2)$, of roughly 10^3 cm^{-3}. The chemistry will be described in more detail in the following section.

We assumed that initially 0.96 $M_\odot$ of gas was distributed in a sphere at a uniform $n=n_0=2.8\times10^3$ cm^{-3} and $T=10$ K. The mass fraction of He was taken to be 0.2. A modified free-fall collapse to a truncated singular isothermal sphere was assumed to ensue. The density profile of this intermediate configuration falls as r^{-2}, where r is the radial distance from the centre. At the outer boundary of $r_c=1.58\times10^{17}$ cm, n was taken to be 1.86×10^4 cm^{-3}, which is typical of the NH_3 emission regions in L1498 (Myers & Benson 1983). The mass of this configuration marginally exceeds that of an equilibrium, static, truncated, singular isothermal sphere with the assumed temperature, composition and truncation radius. The motivation for the assumption, that the initial phase of collapse proceeds in this fashion and results in such a configuration, will be apparent to someone who has studied Shu (1977).

We assumed that the singular isothermal configuration is established by parcels of gas collapsing to a range of values of n_f, the final number densities to which the modified free-fall collapse brings them. After a parcel reaches the n_f appropriate for its radial position in the truncated singular isothermal sphere, its density is assumed to remain fixed until all of the gas interior to it has collapsed to the desired configuration and a collapse-expansion wave (CEW), propagating outwardly in a self-similar fashion governed by Shu's (1977) solution, reaches the parcel which then begins to fall inwardly. The CEW is really a pressure wave, propagating at the isothermal sound speed (0.198 km s^{-1} in our work), and collapse from the initial singular configuration does not occur exterior to it, simply because external material has not 'felt' the pressure drop created by the infall of internal material.

The modified free-fall collapse to a particular n_f was taken to proceed according to (Spitzer 1978; Nejad *et al.* 1990):

$$\frac{dn}{dt}=B\left(\frac{n^4}{n_0}\right)^{1/3}\left\{24\pi G m_H n_0\left[\left(\frac{n}{n_0}\right)^{1/3}-1\right]\right\}^{1/2}, \qquad n>n_0, \quad (1)$$

where t, G and m_H are time, the gravitational constant, and the mass of a hydrogen atom. B may be thought of as a retardation factor which will have a density-dependent value less than 1.0 when the effects of magnetic and rotational support are manifest. To permit easy comparison with earlier published results we set $B=0.7$. (This value was used in our previous work on dynamical and chemical cycling in low-mass star-forming regions, since it resulted in the collapse

from the specified initial density to the specified final density requiring almost 1.0×10^6 yr, a convenient time-scale.)

The observations indicate that the chemistry is 'young'. Therefore, we assume that immediately following the establishment of the singular isothermal configuration, the self-similar collapse (Shu 1977) of that structure begins. Outside of the CEW the material is static with $n \propto r^{-2}$. Inside the CEW, matter approaches free-fall with $n \propto r^{-3/2}$ and $v \propto r^{-1/2}$, where v is the infall speed. There is a smooth transition from subsonic to supersonic flow near the edge of the CEW. The position of the CEW is a direct measure of the collapse age and the proportion of the cloud that has begun to collapse. At any one time, about 49 per cent of the mass within the CEW is concentrated in a central, nearly hydrostatic core which is surrounded by an infalling envelope interior to the quiescent ambient globule. Note that we are concerned specifically with the behaviour of the material in the outer parts of the envelope ($r = 10^{15}$ to 1.58×10^{17} cm and $n \approx 10^7$ to 1.86×10^4 cm^{-3}) and do not address the problem of the formation of a stellar core.

We have adopted the model of Shu (1977) rather than that of Larson (1972) for several reasons. First, the observations [by Myers & Benson (1983) and others] suggest that the globules sit in the $n \propto r^{-2}$ state for some time before collapse initiates. Larson's models [as well as the more complex models of Winkler & Newman (1980a,b)] start with an isothermal ($T = 10$ K), homogeneous sphere. This might not be expected to be a problem, since the homogeneous sphere quickly relaxes to the $n \propto r^{-2}$ state, and (as Shu pointed out), the density and velocity profiles in Shu's fig. 3 are very similar to those in Larson's fig. 10 except for the detailed behaviour at the head of the expansion wave. However, this behaviour can significantly affect the shape of the calculated line profiles.

Secondly, while Shu was concerned with the isothermal collapse phase, Larson focused more on the physical conditions some time after the formation of a stellar core. In these situations an isothermal structure does not obtain, and the temperature is roughly proportional to $r^{-1/2}$. Larson's 1972 paper differs from his 1969 paper principally in that results for a wider range of cloud masses were presented and a more accurate treatment of the radiative transfer was employed. This results in an asymptotic temperature dependence of $T = 2.5 \times 10^9\ r^{-1/2}$ K (r in cm) at the time when about half of the mass has collapsed into the protostellar object. Thus $T \approx 10$–20 K at 10^{17} cm and ≈ 80–100 K at 10^{15} cm. The precise temperature structure depends on the assumed opacity law. However, such large temperature variations at these radii are incompatible with the detailed studies of Winkler & Newman (1980a,b), who identified an initial isothermal collapse phase which results in the formation of an opaque stellar core at $r \approx 10^{14}$ cm when the central density reaches 10^{-13} g cm^{-3}. There then follows a lengthy accretion phase lasting some nine orders of magnitude longer than the initial collapse phase. From fig. 4 of Winkler & Newman (1980b) it can be seen that the outer envelope ($r > 10^{15}$ cm) is isothermal for much of the early stages of the evolution, and [from fig. 6d of Winkler & Newman (1980b)], that even near the end of the main accretion phase the radiation temperature is only about 35 K at 10^{15} cm. Observational constraints on any significant increase in temperature with decreasing radius are set by the narrowness of the NH_3 lines; we argue that depletion contributes to their narrowness, but if T were as high as, say, 100 K, NH_3 would evaporate from mantles back into the gas phase. We have allowed for a possible power-law variation of temperature, so as to test the chemical sensitivity to temperature.

Thirdly, Shu's model gives the time dependence of the density and velocity profiles. As the solutions are self-similar (with a similarity variable $x = r/c_s t_c$, where c_s is the isothermal sound speed and t_c is the time that has elapsed since the CEW began to propagate outwardly), the profiles can easily be scaled to describe any particular cloud mass or collapse age. The self-similar nature of the solutions for $v(r, t)$ and $n(r, t)$ makes them computationally easy to apply.

There are, however, some limitations in the approach of Shu. These are briefly listed here. (i) The behaviour of the CEW when it reaches the outer boundary (at $t_c \approx 8 \times 10^{12}$ s in the standard 0.96-$M_\odot$ model) is uncertain. Near this boundary the similarity solution breaks down as a compression wave will form at the boundary, steepening into a shock wave as it moves into the interior. (ii) The very nature of the boundary is uncertain. For most models it is assumed to be fixed in space and that a non-varying pressure is maintained at it. Shu's model shows that the outcome of the collapse is critically dependent on the assumed boundary conditions. (iii) The process by which the truncated isothermal sphere is formed and the length of time that it spends in this state are uncertain. These are major problems, especially when one is trying to establish the chemical conditions immediately prior to the onset of the collapse of the truncated singular isothermal spheres. (Internal conditions are discussed in more detail in the next section.) (iv) Finally, it should be noted that magnetic retardation of the collapse has not been included in the model.

However, our goal is to identify species with broad emission lines which will enable us to diagnose the nature of the boundaries and the detailed behaviour of the CEW. For our purposes, Shu's work provides as reliable a description of reality as can be meaningful until the sorts of observational diagnostics that we are considering are actually utilized.

2.2 Some details of the calculations

The physical parameters that we have used in our standard model are given in Table 1. We will focus on L1498, which is a starless core, because no perturbation of the line profiles due to an outflow–ambient-medium interaction occurs. Its mass may be somewhat less than that which we adopt for our

Table 1. Physical parameters of the globule as used in the model.

Total mass	=	0.96 $M_\odot$
Extinction (A_v)	=	8.0 mag.
Temperature	=	10 K
Truncation radius (r_c)	=	1.58×10^{17} cm
Time at which CEW reaches r_c	=	8.0×10^{12} s
Hydrogen nucleon number density at r_c	=	1.86×10^4 cm

models, but the observational estimates of masses are always sufficiently uncertain that this discrepancy between model and observationally derived masses is unimportant. Furthermore, if depletion is important the observational estimate of the mass of L1498 will be too low in any case.

The number density and infall velocity are continually varying functions of r and t_c. The time-scale for collapse is similar to that for freeze-out. Therefore, to calculate the chemical abundances at any position and any time, it is necessary to follow the time-dependent chemistry and physical conditions of a parcel of gas until its motion brings it to the spatial position and time being considered. To obtain the chemical abundances as functions of radius at any one time, it is necessary to perform integrations for many parcels of gas distribution at that one time over the range of radii of interest. In practice, the motions and physical and chemical evolutions of up to 100 parcels of gas were followed in each run. To calculate line profiles we need to know the abundances at a number of radial points at the same specified time. Parcels of gas were distributed intially in such a way that at the time for which the line profiles were calculated, the parcels were distributed uniformly in r. The mass in a parcel is proportional to the product of r^2 with the density (at r) at the time at which the profile is formed; hence the masses of the parcels are not equal to one another since the density ceases to have a simple r^{-2} behaviour after the CEW has begun to move outwardly.

We consider no models for $t_c > 8\times10^{12}$ s, due to the uncertainty in the structure of the CEW resulting from poor knowledge of boundary. The following assumptions and procedures were adopted.

(i) The lines were taken to be optically thin so that contributions to the emission profiles can simply be added. Many lines will, in fact, be optically thin. We underestimate the ratio of the line-wing to line-core strengths by making the assumption of optical thinness. In particular, the $NH_3(1,1)$ line has an optical depth greater than unity; nonetheless, the observed line in L1498 does not possess strong wings.

(ii) Line broadening by systematic motion and by turbulence has been included. The possibility that the temperature varies as a power law of the radius was considered in the chemistry and included in the summation of contributions from different radii, but the effect of such a temperature variation was not included in the dynamical description of the collapse. The possibility of a turbulent velocity dispersion that depends on the infall velocity was also considered in the summation, but its effect was also not included in the dynamical description of the collapse. The turbulent velocity dispersion in the subsonic part of the flow was set constant, but was assumed to be damped very rapidly in the supersonic region. A turbulent velocity dispersion of about 0.065 km s^{-1} in the subsonic region of Shu's solution is required to fit the core of the NH_3 profile of L1498 (Myers & Benson 1983).

(iii) We have assumed Gaussian beams with half-power widths determined by the telescope parameters and the wavelength of the line being observed. For the $NH_3(1,1)$ line we have used the same parameters as Myers & Benson. The details are summarized in Table 2. In all cases we have assumed that the beam is centred on the collapse core.

(iv) In calculating the profiles we performed a spherical integral over the range $r = 10^{15}$ to 1.58×10^{17} cm and $n = 10^7$ to 1.86×10^4 cm^{-3}. The contributions to the profile rapidly diminish at higher densities and smaller radii, and the calculations (for the abundances as well as the profiles) were halted when the velocity reached 1 km s^{-1}. Even the broadest profiles have narrower widths than this.

(v) It is assumed that the material outside the globules has negligible density and does not contribute to the profile.

3 THE CHEMISTRY AND INITIAL CONDITIONS

3.1 The chemistry

For the sake of consistency we have adopted a chemical scheme similar to that used in a previous study of nitrogen chemistry where depletion has been included (Nejad *et al.* 1990). Thus, we follow the time-dependent abundance of electrons and 85 other species containing H, He, C, N, O, S and Na, a representative heavy metal important for establishing the gas-phase ionization structure. The species list is limited to small molecules of four atoms or less (e.g. H_2CO^+). Depletion of all elements except H, He and Na increases with time, but we include no desorption mechanism for molecular species from the solid state, except when adopting the initial conditions. Our chemistry consists of 1147 reactions in a closed network. The rate-file, though largely similar to that used by Nejad *et al.* (1990), has been updated with data in RATE90 [the latest UMIST rate-file database; see Millar *et al.* (1991) for precise details]. This has altered the rate coefficients of about 30 reactions, including some affecting the nitrogen chemistry and several low-temperature reactions involving oxygen. The two reactions:

$$O + OH \longrightarrow O_2 + H,$$

$$O + CH \longrightarrow CO + H,$$

are believed to be fast at low temperatures (Graff 1989) and could severely inhibit the hydrocarbon chemistry. The H_3O^+ dissociative-recombination branching ratio in RATE90 differs significantly from that used by Nejad *et al.*

3.1.1 *Photoreactions*

Most of the clouds that have been observed have intermediate to large extinctions: L1498 has an extinction $A_V \simeq 5$–6 (Myers & Benson 1983; Benson & Myers 1983; with an H_2 column density of 5.0×10^{21} cm^{-2} deduced from CO observations), L1551 has $A_V \simeq 10$ and the 'mean core' of Myers & Benson's survey has $A_V \simeq 18$. Thus the cosmic-ray-induced photodissociation mechanism discussed by Prasad & Tarafdar (1983) is likely to be important and has been included in our calculations. Cosmic rays (10–100 MeV) penetrate dark clouds, ionizing H_2 and generating secondary electrons (with energies ~30 eV). These electrons excite electronic states of H_2, the decays of which produce an ionizing/dissociating UV flux. The rates for these processes are given by

$$R = \zeta_{cr} P(i)\, n(i) \left(\frac{1}{1-\omega}\right) \text{cm}^{-3}\,\text{s}^{-1},$$

where ω is the grain albedo, ζ_{cr} is the cosmic-ray ionization

Table 2. Parameter values adopted for the different runs.

Free-fall retardation factor (B)	= 0.7
Sticking coefficient (S_i)	= 1/3 (neutral species)
	= 1 (positive ions)
Grain albedo	= 0.5
Cosmic ray ionization rate (ζ_{cr})	= 5.0×10^{-18} s^{-1} (D=1)
	= 3.0×10^{-18} s^{-1} (D=2)
	= 1.5×10^{-18} s^{-1} (D=3)
Assumed distance	= 140 pc

Line	HPBW	Projected HPBW	Telescope
NH_3(1,1) 23.7 GHz	1′.4	1.76×10^{17} cm	37 m Haystack
NH_3(1,1) 23.7 GHz	40″	8.38×10^{16} cm	100 m Bonn
CH 3.3 GHz	4′.0	5.03×10^{17} cm	100 m Bonn
H_2S 169 GHz	35″	7.33×10^{16} cm	30 m IRAM
HCO 86.67-86.80 GHz	29″	6.08×10^{16} cm	30 m IRAM
HCO^+ 89.2 GHz	28″	5.89×10^{16} cm	30 m IRAM
N_2H^+ 93 GHz	27″	5.66×10^{16} cm	30 m IRAM

Depletion coefficient, D, and collapse ages ($t_c \times 10^{12}$ s), and turbulent r.m.s. velocity dispersions, V_{TURB}

Model 1	D=1	t_c=8	V_{TURB} = 0.037 Km s^{-1}
Model 2	D=2	t_c=8	V_{TURB} = 0.037 Km s^{-1}
Model 3	D=3	t_c=8	V_{TURB} = 0.061 Km s^{-1}
Model 4	D=1	t_c=6	V_{TURB} = 0.079 Km s^{-1}
Model 5	D=2	t_c=6	V_{TURB} = 0.079 Km s^{-1}
Model 6	D=3	t_c=6	V_{TURB} = 0.079 Km s^{-1}
Model 7	D=1	t_c=4	V_{TURB} = 0.083 Km s^{-1}
Model 8	D=2	t_c=4	V_{TURB} = 0.083 Km s^{-1}
Model 9	D=3	t_c=4	V_{TURB} = 0.083 Km s^{-1}

rate, $n(i)$ is the number density (cm^{-3}) of species i and $P(i)$ represents an integration of the cross-section for the process over the UV spectrum. In our standard model we assume that $\omega = 0.5$ and $\zeta_{cr} = 5.0 \times 10^{-18}$ s^{-1}. Values for $P(i)$ were taken from Gredel *et al.* (1989), Gredel (1990), Sternberg, Delgarno & Lepp (1987) and, for the case of CO, Gredel, Lepp & Dalgarno (1987). These values are for a grain cross-section per hydrogen nucleus of 2.0×10^{-21} cm^2. CO is a little unusual in that it dissociates following absorption in discrete lines. P(CO) is therefore a function of the CO abundance and temperature. For $x(CO) \sim 7.5 \times 10^{-5}$ and $T = 10$ K, $P(CO) = 4$. Where $P(i)$ is not tabulated a value of 200, which is typical for molecular dissociation by continuum radiation, is assumed. In addition to cosmic-ray-induced photodissociation we have also included the effect of external UV penetrating into the clumps, although its significance is only marginal, and for $A_V > 10$ it is negligible.

3.1.2 *Freeze-out reactions*

Following Spitzer (1978) and Umebayashi & Nakano (1980), the rate per unit volume at which a species freezes out is

given by

$$\frac{dn(i)}{dt} = 4.57\times10^{4}\, d_g a^2 T^{1/2} C n S_i m_i^{-1/2} n(i)\ \mathrm{cm^{-3}\ s^{-1}}, \qquad (2)$$

where d_g is the ratio of the number densities of grains to hydrogen nuclei, a is the grain radius in cm, S_i is the sticking coefficient (in the range 0 to 1), m_i is the molecular mass of species i in amu and C is a factor which takes into account electrostatic effects. For the temperatures and densities encountered in dark globules, the average grain charge is about -1 (Umebayashi & Nakano 1980), in which case

$$C = \begin{cases} 1 & \text{for neutral species,} \\ 1+(16.71\times10^{-4}/aT) & \text{for singly charged positive ions.} \end{cases}$$

Thus the ionic species will freeze out faster than the neutrals by a factor of order 10 (for $a = 10^{-5}$ cm). The quantity $\pi d_g a^2$ can be thought of as the grain surface area per hydrogen nucleon. In reality there is more than one grain population and this quantity should be averaged over the grain size distribution. Since the size distribution is unknown we can only estimate this value and leave it as the main free parameter of the model. If we assume a typical Mathis, Rumpl & Nordsieck (1977) power-law size distribution of grains with normal characteristics, we obtain

$$\langle d_g a^2\rangle \approx 2.6\times10^{-22}\ \mathrm{cm^2}.$$

This compares very well with the value of 2.2×10^{-22} cm^2 used by Nejad *et al.* (1990).

In our model we have used

$$\langle d_g a^2\rangle = D(2.2\times10^{-22}\ \mathrm{cm^2}),$$

where the depletion coefficient, D, is either 1.0, 2.0 or 3.0. The value of D depends on the abundance of very small grains (*cf.* Duley & Williams 1984). In the expression for C we have used $a = 1.0\times10^{-5}$ cm, though this could be somewhat smaller for the Mathis *et al.* distribution. Laboratory measurements and quantum-mechanical calculations (Leitch-Devlin & Williams 1985) suggest that $S_i \sim 0.1$–1.0 for all species interacting with realistic grain materials. We assume that hydrogen atoms sticking to grains combine to form H_2 which is then immediately ejected back into the gas phase. Thus, the implied H_2 formation rate depends on the assumed grain properties. It is also assumed that electrons impinge upon and stick to grains at a rate that is just sufficient to neutralize all accreted ionic species. He^+ and Na^+ ions that collide with grains are assumed to return to the gas phase as neutral He and Na, which with H_2 are assumed to be inert with respect to grains.

3.2 The initial conditions

It is necessary to establish the chemical conditions prior to cloud collapse. The model results presented for the velocity distributions of chemical species are for times after which the CEW has begun to propagate outwardly through the singular isothermal sphere. During the CEW propagation, depletion reduces $x(NH_3)$ in gas at $n \approx 1.86\times10^4$ cm^{-3}, from which the bulk of the emission arises, by a factor of about $\exp(-Dt_c/2.4\times10^{13}\ \mathrm{s})$ with respect to its value when the CEW first began to propagate outwardly (i.e. when $t_c = 0$). For our models this factor is between 0.86 and 0.37. Given that the factor is of order unity, that uncertainties in the determination of $x(NH_3)$ and other parameters for L1498 from observations exist, and that our primary goal is to identify species that are likely to have broad emission wings rather than to create models from existing data for such species, we attempted only to ensure that the model values of $x(NH_3)$ (at $t_c = 0$ and $n = 1.86\times10^4$ cm^{-3}) were within 20 per cent of the measured value of $x(NH_3) \approx 8\times10^{-8}$ (Benson & Myers 1983) for L1498.

We achieved approximate agreement between the measured value and the model value (at $n = 1.86\times10^4$ cm^{-3} and $t_c = 0$) of $x(NH_3)$, by taking the chemical abundances given by Nejad *et al.* for the post-shock gas at $n = 2.8\times10^3$ cm^{-3} immediately after its temperature has fallen to 10 K at the beginning of the third dynamical cycle of their cyclic dynamical–chemical model for B5. This initial state is then evolved according to our chemistry, with appropriate combinations of D and ζ_{cr} during collapse and subsequent steady state. The gas-phase elemental fractional abundances, for the initial chemical conditions adopted for the onset of the modified free-fall collapse governed by equation (1), are given in Table 3. We find, with Nejad *et al.* (1990), that the required high abundances of NH_3 can only be obtained if surface reactions on dust grains act to convert nitrogen atoms into ammonia. Like Nejad *et al.*, we found that the gas-phase elemental abundance of sulphur must be low in order for significant survival of NH_3. It should be noted, however, that there are very significant differences between the results of our model and those of Nejad *et al.* (1990). These are almost entirely due to the effects of cosmic-ray-induced photodissociation which was not included by Nejad *et al.* (1990).

Acceptable combinations of D and ζ_{cr} are constrained by the requirement that depletion and cosmic-ray-induced photodestruction reduce the high gas-phase fractional abundance, at the onset of the modified free-fall collapse, to the measured value. The effect of depletion on the NH_3 abundance was discussed in the first paragraph of this subsection. The cosmic-ray-induced photodestruction of NH_3 occurs on a time-scale of roughly $(2200\ \zeta_{cr})^{-1}$ s. Since

Table 3. Total gas-phase elemental abundances relative to hydrogen at the start of the initial collapse phase.

H:	1.0
He:	0.0763
C:	3.75×10^{-4}
N:	1.15×10^{-4}
O:	6.755×10^{-4}
Na:	2.2×10^{-7}
S:	1.6×10^{-6}

the modified free-fall collapse requires 10^6 yr, $\zeta_{cr} \lesssim 10^{-17}$ s^{-1} in order for cosmic-ray-induced photodestruction to have a limited effect on the gas-phase abundance of NH_3. Clearly, if a configuration like the singular isothermal sphere were maintained for several million years, by magnetic support, say, D and ζ_{cr} would have to be reduced from the values that we have used.

Examples of the chemical results (as fractional abundances relative to the total hydrogen nucleon density n), obtained for a parcel of gas that experiences modified free-fall collapse and remains at fixed density, are given in Fig. 1 (for which $B = 0.7$, $n_f = 1.86 \times 10^4$ cm^{-3}, $\zeta_{cr} = 5.0 \times 10^{-18}$ s^{-1} and $D = 1.0$). The decrease of many abundances at times of $2-3 \times 10^6$ yr as depletion becomes greater, and the increases in other abundances, are clearly seen. Initially, the overabundance, relative to steady state, of NH_3, H_2O and other saturated molecules results in the breakdown of such species, in reactions with ions or following photoabsorption,

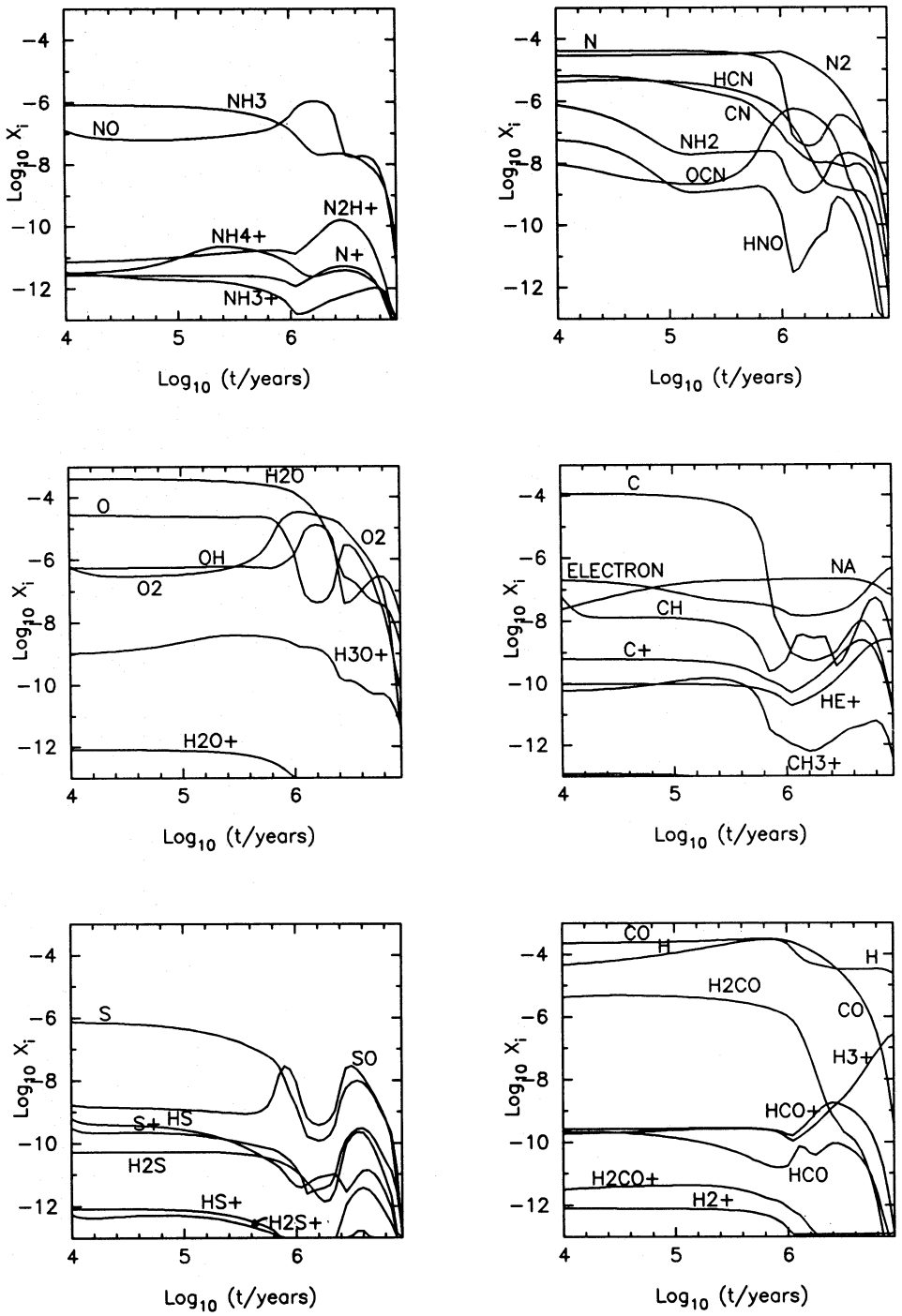

Figure 1. Results for modified free-fall collapse followed by a period at a constant density of $n_f = 1.86 \times 10^4$ cm^{-3}. Abundances of selected species are given as $\log_{10}(x_i)$ where x_i is the fractional abundance of species i relative to hydrogen nucleons by number. Free-fall collapse is halted at $t \sim 1.0 \times 10^6$ yr.

triggering most of the formation of smaller species such as CH and OH. An initiating breakdown reaction remains important for the formation of some species even at late times, but build-up, by ion–neutral reactions, from smaller species becomes increasingly important for the formation of many species. At later times the chemistry is driven to a greater extent by cosmic-ray ionization, as is usual in dark-cloud chemistries.

4 RESULTS

The results from the full collapse models are presented in Figs 2–6. The basic values for the physical parameters used in these runs are given in Table 2. Nine calculations were performed (each taking up to 3 hr CPU time on a VAX 3500) for three depletion rates and three values of the collapse age: 4×10^{12}, 6×10^{12} and 8×10^{12} s, corresponding

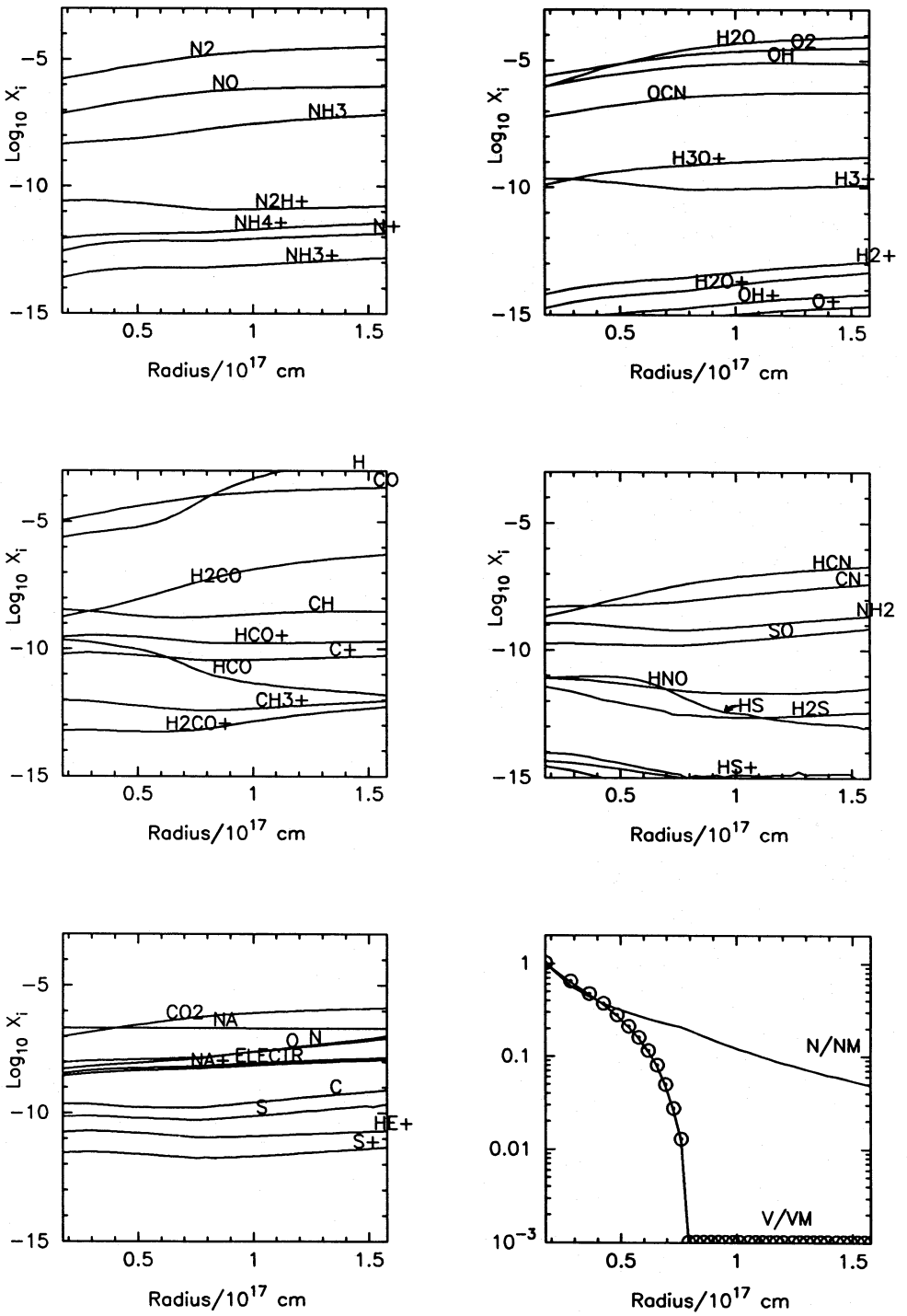

Figure 2. Results from model run no. 7 ($D=1$, $t_c=4\times10^{12}$ s). In addition to the fractional abundances, the density and velocity profiles are shown. The density and velocity are normalized to the maximum value (on the left-hand side). The circles on the velocity curve mark the final positions of the radial grid points.

to about 50, 75 and 100 per cent of the total cloud mass being within the CEW. The spread of depletion rates investigated may seem small, but as the collapse time-scale ($\sim 2.2\times10^5$ yr) is very similar to the freeze-out time-scale ($6.6\times10^5\ D^{-1}$ yr for NH_3 at $n=1.86\times10^4$ cm^{-3}), the chemical behaviour was found to be critically dependent on the depletion rate.

In order to maintain the NH_3 abundance (until the singular isothermal configuration is established) at a value that is compatible with the observations, it was also necessary to alter slightly ζ_{cr} in conjunction with the depletion rate. The values used are given in Table 2 and resulted in shifts of the NH_3 abundance by less than 20 per cent.

Fig. 2 presents the results obtained from run number 7 ($D=1$, $t_c=4\times10^{12}$ s). As with the modified free-fall results in Fig. 1, the fractional abundances (for selected species) are given by number relative to hydrogen nucleons. Integrations were performed for each radial point shown in Fig. 2 in three distinct phases: collapse to the singular isothermal sphere followed by immediate initiation of the CEW at the centre;

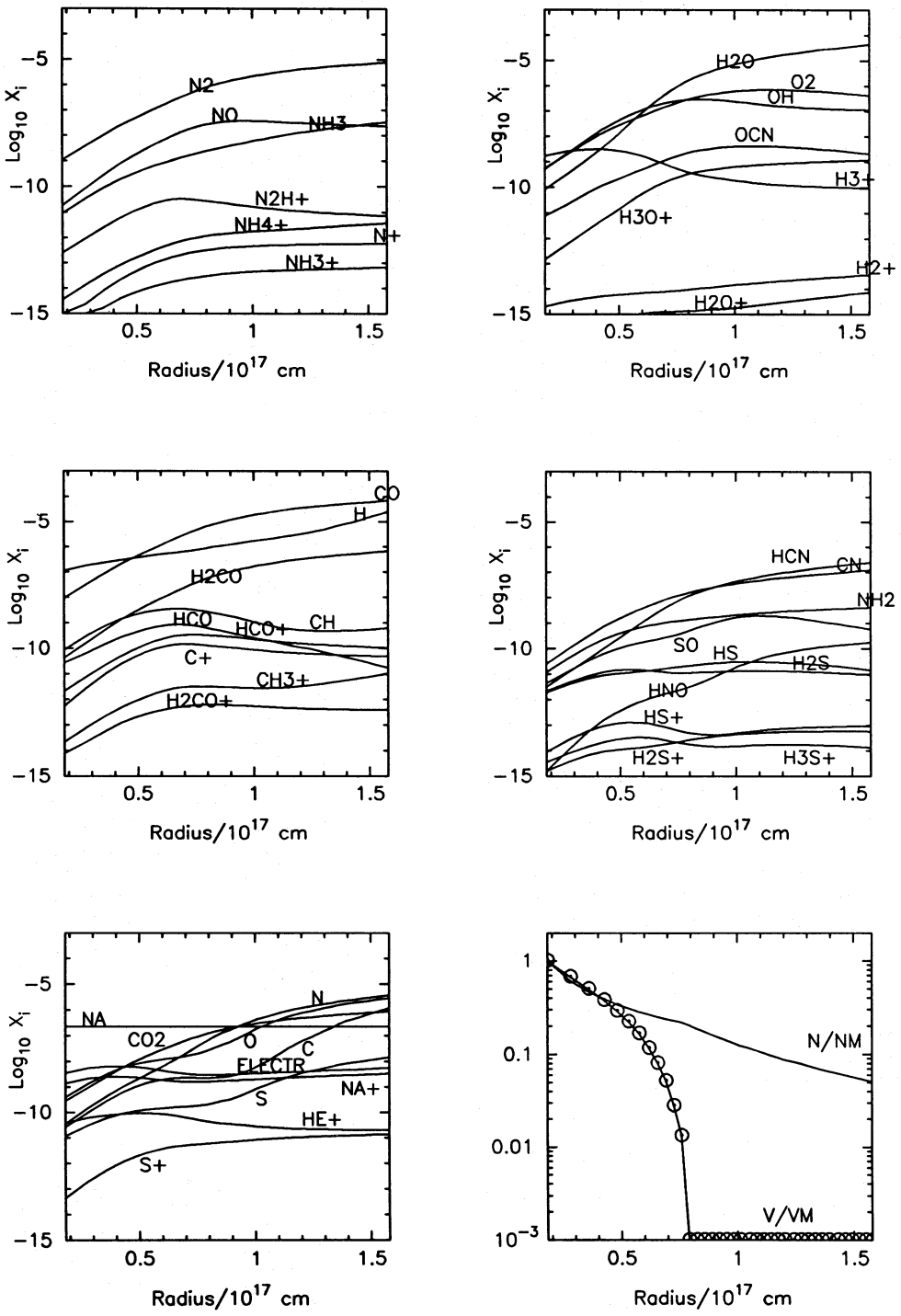

Figure 3. As Fig. 2, only for run no. 9. This differs from run no. 7 only in that the depletion rate is three times larger.

chemical evolution in the hydrostatic sphere before the arrival of the CEW; and dynamical evolution once the matter is overtaken by the CEW.

In Fig. 2 the increases, with progressively smaller radius, of the abundances of some species, such as CH and H_2S, are particularly noticeable when compared to the steady decline of the NH_3 as it freezes out. Species showing significant enhancement as the inflow progresses, in this and other runs, are CH, HCO, HNO, N_2H^+, HCO^+, HS and H_2S. Distinct enhancements are also seen in OH, NH_2, OCN and SO. The velocity and density profiles are also presented in Fig. 2 and show the characteristics of the CEW; one sees the change of the density profile from a r^{-2} law (static) to a $r^{-3/2}$ law (free-fall) and the smooth acceleration of the inflow through the sonic point. The final distribution of the radial grid points is shown by circles on the velocity curve.

In Fig. 3 we present the results obtained from run number 9 which is similar to run 7 except that the depletion coefficient, D, has been increased from 1 to 3. Comparing these two figures we can see the extreme sensitivity of the chemistry to the depletion rate; a factor of 3 increase in D can result in abundance variations of several orders of magnitude at radii less than a few times 10^{16} cm. The importance of this behaviour becomes apparent from the appearance of the line profiles. In Fig. 4 we present the results, for all nine runs, for the 10 species other than NH_2 most likely to have broad velocity distributions. The sensitivity of the chemical behaviour to the collapse age and the depletion rate is clearly apparent (e.g. compare the results from run 1 to those from run 9).

The calculated profiles for NH_3, CH, H_2S, HCO, HCO^+ and N_2H^+ are shown in Fig. 5 for each of the nine runs, together with the NH_3 profile as observed by Myers & Benson (1983). In calculating these profiles we have (initially) assumed a turbulent velocity of zero. However, all of the NH_3 line profiles are slightly narrower than the observed line (particularly runs 4 to 9). Thus we have 'bulked out' all of the profiles in our calculations by the addition of a constant turbulent velocity dispersion (V_{TURB}), chosen to give a good match between theoretical and observed NH_3 line cores. The adopted values of V_{TURB} are given in Table 2. The telescope parameters (and hence the angular resolution) for each of the observed lines are also presented in Table 2. For the case of the $NH_3(1,1)$ line we have performed calculations for the 37-m Haystack telescope (which was used by Myers & Benson) and also for the 100-m Bonn telescope. The effect of the higher resolution that can be obtained with the 100-m telescope is immediately obvious; the enhanced line broadening should be clearly visible and strongly position dependent. The resolution for CH line observations is about 4.0 arcmin with the Bonn telescope, but broad line wings would be much more likely to be seen with the Very Large Array (VLA) or with the Arecibo telescope, if they were equipped with the necessary receivers. The other species emit at frequencies which should be detectable with the 30-m IRAM telescope (i.e. in the range 83–270 GHz).

In general it can be seen that we get excellent agreement with the observed NH_3 line profile for most of the cases studied. Runs 1 to 3 demonstrate slight NH_3 wing excesses which, given the observational uncertainties, are probably in harmony with the data. The chemical reasons for the CH, HCO^+, HCO, H_2S and N_2H^+ having particularly broad lines are straightforward. The formation of CH is initiated by the reaction

$$He^+ + CO \longrightarrow C^+ + O + He.$$

Since that reaction is the primary removal mechanism of He^+, the formation rate of C^+ is initially insensitive to the depletion. However, as the depletion increases, the probability grows that C^+ will react with H_2, rather than with an oxygen-bearing species leading to the re-formation of CO. Thus, the formation rates of CH_2^+ and of species whose formation sequences involve reactions including CH_2^+ increase with depletion. CH is such a species. Furthermore, CH is removed primarily in reactions with oxygen-bearing species, the abundances of which decrease with rising depletion; therefore the CH removal rate declines as depletion grows.

A major removal mechanism for HCO^+ is the reaction

$$HCO^+ + H_2O \longrightarrow H_3O^+ + CO.$$

As depletion occurs, the H_2O gas-phase abundance decreases resulting in a significant decrease in the removal rate of HCO^+. When the depletion is greater, HCO^+ is removed primarily by dielectronic recombination and its fractional abundance drops with increasing depletion and density. HCO is formed primarily by the reaction

$$HCO^+ + Na \longrightarrow HCO + Na^+.$$

Hence, the HCO formation rate follows the HCO^+ abundance. HCO is removed mostly in reactions with atomic hydrogen, the number density of which is roughly independent of n (see, e.g., Duley & Williams 1984), since the formation rate per unit volume of H scales with $\zeta_{cr}\, n$ and the removal of H, by its conversion to H_2 on grain surfaces, has a rate per unit volume that also scales with n. Since the removal time-scale of HCO is approximately constant, the HCO-to-HCO^+ abundance ratio is expected to scale roughly as n.

The depletion time-scale for nitrogen is roughly the same as that for oxygen, and the N_2 abundance follows that of CO. Consequently, just as the product $n(CO)\,n(H_3^+)$ is roughly constant with depletion (since the reaction of H_3^+ with CO is a major removal mechanism for H_3^+), the product $n(N_2)\,n(H_3^+)$ does not vary greatly with depletion. Thus, the formation rate per unit volume of N_2H^+, by

$$N_2 + H_3^+ \longrightarrow N_2H^+ + H_2,$$

is insensitive to depletion. A major removal mechanism for N_2H^+ is the reaction between it and H_2O. The drop in the gas-phase water abundance with increasing depletion results in a rising N_2H^+ fractional abundance until its reaction with electrons greatly dominates its removal.

The depletion rate of atomic sulphur is similar to that of CO. Hence, the formation rate of HS^+ per unit volume, by

$$S + H_3^+ \longrightarrow HS^+ + H_2,$$

is roughly independent of depletion. HS^+ reacts slowly with H_2:

$$HS^+ + H_2 \longrightarrow H_3S^+ + h\nu,$$

which leads to the formation of H_2S. It also reacts with H_2O which prevents H_2S formation. Clearly, an increase in depletion raises the probability that HS^+ will react with H_2 rather

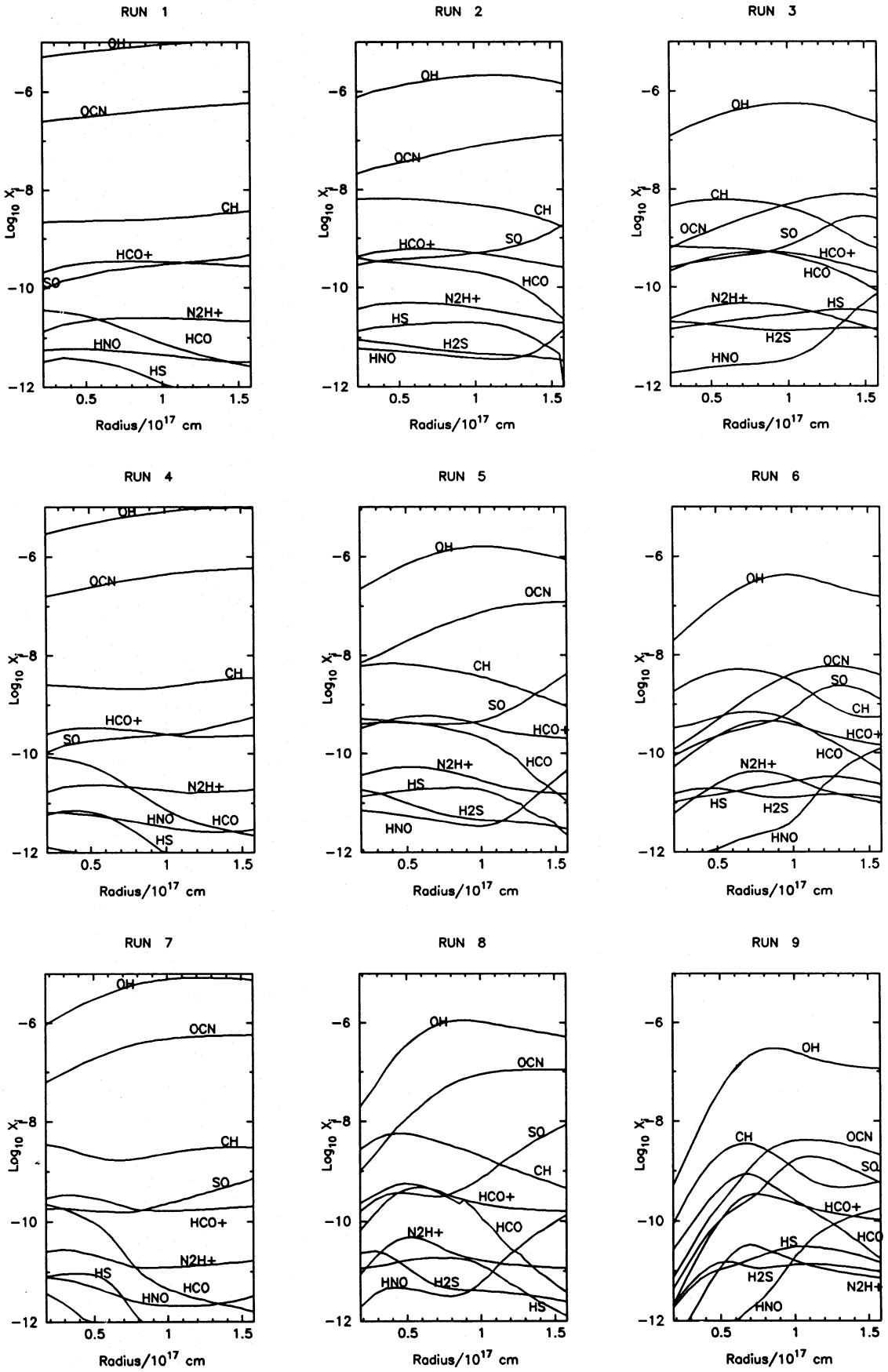

Figure 4. Summarized results from all nine runs. Abundances are given for the 10 (most abundant) species that are likely to demonstrate line broadening as a result of inflow/depletion effects.

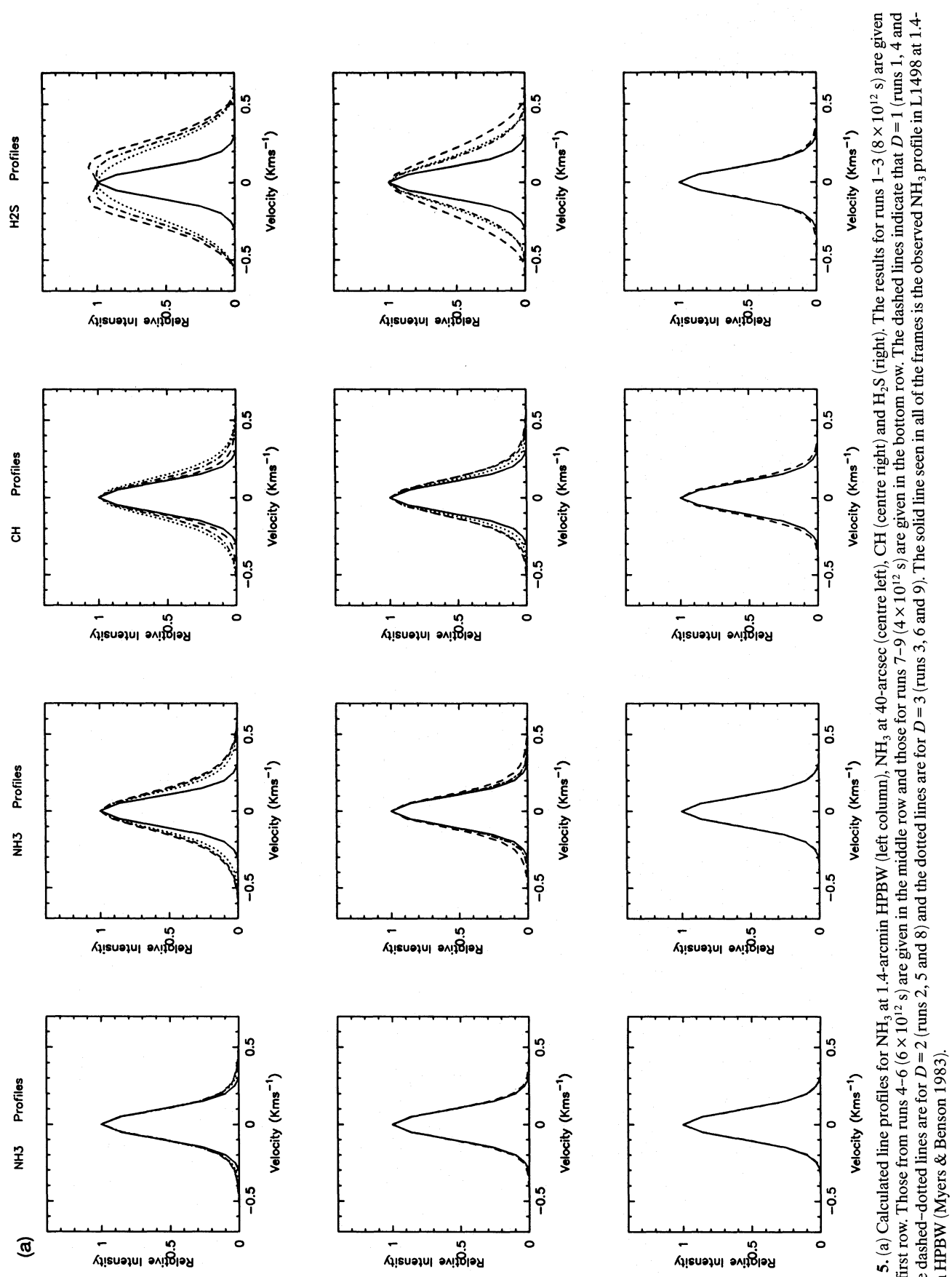

Figure 5. (a) Calculated line profiles for NH_3 at 1.4-arcmin HPBW (left column), NH_3 at 40-arcsec (centre left), CH (centre right) and H_2S (right). The results for runs 1–3 (8×10^{12} s) are given in the first row. Those from runs 4–6 (6×10^{12} s) are given in the middle row and those for runs 7–9 (4×10^{12} s) are given in the bottom row. The dashed lines indicate that $D = 1$ (runs 1, 4 and 7). The dashed–dotted lines are for $D = 2$ (runs 2, 5 and 8) and the dotted lines are for $D = 3$ (runs 3, 6 and 9). The solid line seen in all of the frames is the observed NH_3 profile in L1498 at 1.4-arcmin HPBW (Myers & Benson 1983).

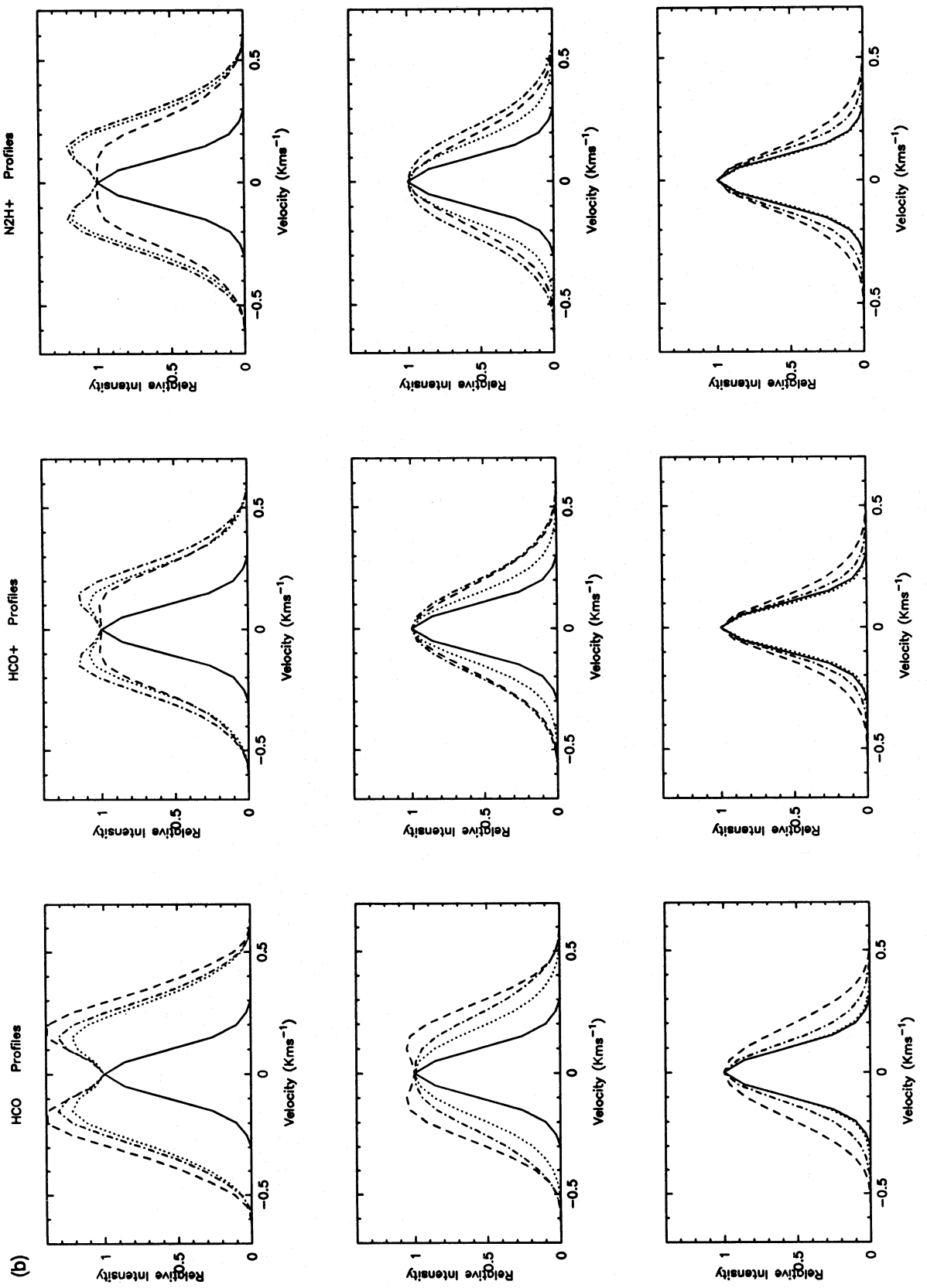

Figure 5. (b) As for (a). Calculated line profiles for HCO (left), HCO^+ (centre) and N_2H^+ (right).

than H_2O. Hence, the H_2S formation rate per unit volume increases with depletion. Its removal rate, due to reactions with ions having number densities that scale with the depletion, increases in about the same way with depletion as its formation rate does. Hence, the H_2S abundance should be approximately independent of depletion, until the depletion becomes sufficiently high that the reaction of HS^+ with electrons is a much more important loss mechanism than is the reaction with H_2O.

In addition to studying the effects of varying the depletion rate, the cosmic-ray ionization rate (ζ_{cr}) and the age of the collapse, we have also investigated the sensitivity of the chemistry to the temperature profile [$T(r)$] and the density and velocity profiles [$n(r)$ and $v(r)$].

For a given density and dynamical structure, the chemical results are insensitive to the assumed temperature profile. (Of course, in reality the temperature structure is important for the dynamics.) In addition to the isothermal cases for which results are given in Figs 2–5, we have considered models in which $T \propto r^{-0.5}$ with $T = 10$ K at the outer edge of the cloud. Despite the rise in temperature at small radii ($T \sim 36$ K at $r \sim 1.23 \times 10^{16}$ cm) the effect on the chemistry is very small. Some species show slightly different abundances at small radii (e.g. C^+, N^+ within $r \sim 2 \times 10^{16}$ cm, CH within 5×10^{16} cm) but the differences are not sufficient to alter the profile wings significantly. The principal effect is for the line core to be slightly widened (by about 0.05 km s^{-1}). We also performed calculations for the case in which the collapse profiles [$n(r)$ and $v(r)$] are given by Larson's (1972) model and not that of Shu (1977). We used a simple three-part linear fit to the Larson profile and then took this profile to move out through the envelope in a self-similar fashion, exactly as the CEW does in Shu's solution. The results of a analogous calculation to that of run 3 are given in Fig. 6 which shows the velocity and density profiles as well as the deduced NH_3 line profile. The NH_3 profile from the 'standard' run is also shown and it can be seen that the effect of using a different collapse profile is noticeable, implying that line profiles are sensitive diagnostics of dynamics. The similarity solution of Shu gives an NH_3 profile which is a better fit to the observed NH_3 profile. Hence, we present chemical results only for that solution. However, it is clearly obvious that the precise details of the behaviour at the head of the CEW are very important for line profiles.

5 DISCUSSION AND CONCLUSIONS

In the absence of high-quality data for a variety of species in most globules, we will consider observational results for TMC-1 as summarized by Friberg & Hjalmarson (1990). The values of $x(HCO^+)$, $x(CH)$ and $x(N_2H^+)$ for this source are given as 4×10^{-9}, 1×10^{-8} and 2.3×10^{-10} respectively. No detection of HCO in this source has been reported. The models with abundances in most reasonable agreement with these observational results are models 2 and 5, for which the sets of D, t_c are 2.0, 8×10^{12} s and 2.0, 6×10^{12} s, respectively. These are models for which a moderate amount of depletion has resulted in sufficient drops in $x(H_2O)$ for the abundances of key ions to rise at the outer boundary of the truncated isothermal sphere.

For models 2 and 5, lines of HCO^+, CH, N_2H^+, HCO and H_2S have broad wings. However, comparison of the profiles for the two models shows that the breadths and strengths of the wings depend sensitively on t_c, which measures how far the CEW has propagated outwardly into the singular isothermal configuration.

It is probably possible to find combinations of initial chemical conditions, B (the modified free-fall retardation factor), D, ζ_{cr} and t_c that will give fractional abundances of key species in the ranges appropriate for TMC-1 but will also result in no lines having broad wings. However, we are encouraged that the models we have developed give quite naturally the result that NH_3 emission lines should not have broad wings while the lines of a number of other observable species should. Detailed observations of these lines towards a few of the nearest globules will probably provide direct evidence for the infall of protostellar envelopes and allow diagnosis of the dynamics of protostellar collapse.

Stellar outflows or regions in which outflows interact with the ambient gas may also be sources of line wings. However, the species-to-species variations, in contributions to the profile shapes from outflows, would probably be much less

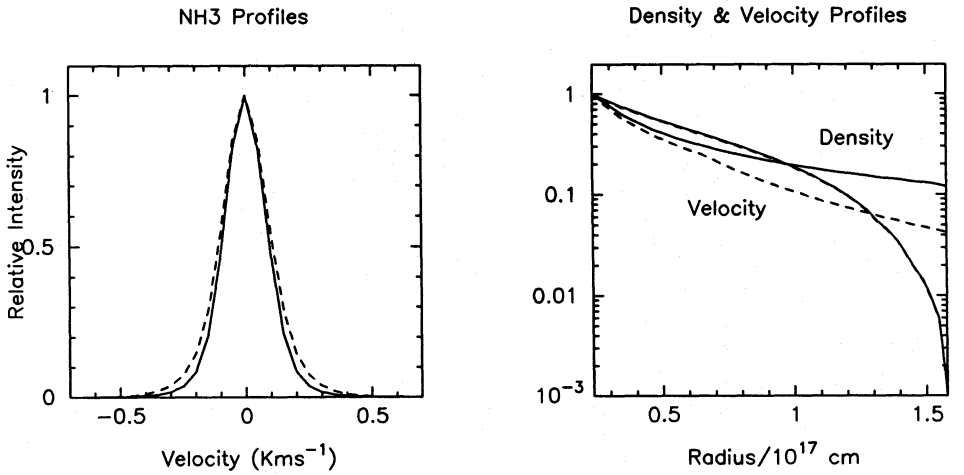

Figure 6. The NH_3 line profile generated with the density and velocity profiles of Larson (dashed lines) and of Shu (solid lines). The assumed HPBW is 1.4 arcmin, the time since the onset of core collapse is 8×10^{12} s and D, the depletion coefficient, is 3.

pronounced than the variations in contributions from infalling gas in which depletion is occurring. Hence, broadening of a line due to infall can in principle be clearly distinguished from broadening due to the presence of outflows.

The advantage of combining high angular resolution with high spectral resolution in studying these line profiles is apparent from the contrast between the model NH_3 line profile for the 100-m telescope and the observed NH_3 line profile obtained towards L1498 with the 37-m telescope.

Several general remarks should also be made about this study. The observed high NH_3 abundances can only be accounted for if gas-phase chemistry is supplemented by grain-surface reactions, with some mechanism of returning the products to the gas, as in Nejad *et al.* (1990). Dark globules are observed to be chemically 'young'; we have inferred that the time spent in the pressure-balanced state is short. The clouds are quiescent; we have inferred that there is no release of molecules from ice mantles to the gas phase. The gas-phase chemistry is sensitive to the cosmic-ray flux, through the induced photodissociation. Near-perfect fits to the NH_3 line profiles have been obtained from the model if a modest degree of turbulence is present. The broad profiles predicted for several other species should be readily detectable. The study of these profiles should provide information on the duration of the singular isothermal state, the age of the collapse, and the depletion rate.

REFERENCES

Benson, P. J. & Myers, P. C., 1983. *Astrophys. J.*, **270,** 589.

Charnley, S. B., Dyson, J. E., Hartquist, T. W. & Williams, D. A., 1988a. *Mon. Not. R. astr. Soc.*, **231,** 269.

Charnley, S. B., Dyson, J. E., Hartquist, T. W. & Williams, D. A., 1988b. *Mon. Not. R. astr. Soc.*, **235,** 1257.

Charnley, S. B., Dyson, J. E., Hartquist, T. W. & Williams, D. A., 1990. *Mon. Not. R. astr. Soc.*, **243,** 405.

Duley, W. W. & Williams, D. A., 1984. *Interstellar Chemistry,* Academic Press, London.

Friberg, P. & Hjalmarson, Å, 1990. In: *Molecular Astrophysics – A Volume Honouring Alexander Dalgarno,* p. 3, ed. Hartquist, T. W., Cambridge University Press, Cambridge.

Goldsmith, P. F., Langer, W. D. & Wilson, R. L., 1986. *Astrophys. J. Lett.*, **303,** L11.

Graff, M. M., 1989. *Astrophys. J.*, **339,** 239.

Gredel, R., 1990. In: *Molecular Astrophysics – A Volume Honouring Alexander Dalgarno,* p. 305, ed. Hartquist, T. W., Cambridge University Press, Cambridge.

Gredel, R., Lepp, S. & Dalgarno, A., 1987. *Astrophys. J. Lett.*, **323,** L137.

Gredel, R., Lepp, S., Dalgarno, A. & Herbst, E., 1989. *Astrophys. J.*, **347,** 289.

Hartquist, T. W. & Williams, D. A., 1989. *Mon. Not. R. astr. Soc.*, **241,** 417.

Larson, R. B., 1969. *Mon. Not. R. astr. Soc.*, **145,** 271.

Larson, R. B., 1972. *Mon. Not. R. astr. Soc.*, **157,** 121.

Leitch-Devlin, M. A. & Williams, D. A., 1985. *Mon. Not. R. astr. Soc.*, **213,** 295.

Mathis, J. S., Rumpl, W. & Nordsieck, K. H., 1977. *Astrophys. J.*, **217,** 425.

Menten, K. M. & Walmsley, C. M., 1985. *Astr. Astrophys.*, **146,** 369.

Menten, K. M., Walmsley, C. M., Krugel, E. & Ungerechts, H., 1984. *Astr. Astrophys.*, **137,** 108.

Millar, T. J., Rawlings, J. M. C., Bennett, A., Brown, P. D. & Charnley, S. B., 1991. *Astr. Astrophys. Suppl.*, **87,** 585.

Myers, P. C. & Benson, P. J., 1983. *Astrophys. J.*, **266,** 309.

Nejad, L. A. M., Williams, D. A. & Charnley, S. B., 1990. *Mon. Not. R. astr. Soc.*, **246,** 183.

Norman, C. A. & Silk, J., 1980. *Astrophys. J.*, **238,** 158.

Prasad, S. S. & Tarafdar, S. P., 1983. *Astrophys. J.*, **267,** 603.

Shu, F. H., 1977. *Astrophys. J.*, **214,** 488.

Spitzer, L., 1978. *Physical Processes in the Interstellar Medium,* John Wiley, New York.

Sternberg, A., Dalgarno, A. & Lepp, S., 1987. *Astrophys. J.*, **320,** 676.

Umebayashi, T. & Nakano, T., 1980. *Publs astr. Soc. Japan,* **32,** 405.

Williams, D. A. & Hartquist, T. W., 1984. *Mon. Not. R. astr. Soc.*, **210,** 141.

Winkler, K.-H. A. & Newman, M. J., 1980a. *Astrophys. J.*, **236,** 201.

Winkler, K.-H. A. & Newman, M. J., 1980b. *Astrophys. J.*, **238,** 311.